NASA Technical Memorandum 4018

Integration Effects of D-Shaped, Underwing, Aft-Mounted, Separate-Flow, Flow-Through Nacelles on a High-Wing Transport

Milton Lamb, John R. Carlson,
and Odis C. Pendergraft, Jr.
Langley Research Center
Hampton, Virginia

National Aeronautics
and Space Administration

Scientific and Technical
Information Division

1987

Introduction

In a continuing effort to reduce the installation drag of nacelle/pylon combinations, several experimental investigations were conducted in the Langley 16-Foot Transonic Tunnel on various nacelle/pylon configurations installed on a high-wing, wide-body transonic transport model. A comparison of the installation drag of aft-mounted, mixed-flow, flow-through nacelles having circular and D-shaped inlets was made in reference 1. It was shown that the D-shaped inlet configuration had lower installation drag. It was also noted in reference 1 that the aft-mounted circular nacelle had lower installation drag than a comparable forward-mounted nacelle. However, the mixed-flow nacelles were considered to be unrealistically long for the transport applications considered. The original nacelles were assumed to be those required for a small STOL transport. Therefore, additional tests were conducted with conventional circular, separate-flow, flow-through, forward- and aft-mounted nacelles (ref. 2). Again, it was shown that the aft-mounted nacelle/pylon had lower installation drag. To complete this study, an experimental investigation was conducted with a D-shaped, aft-mounted, separate-flow, flow-through nacelle.

For the present investigation, a new fan cowl was designed to have the same length and internal areas as the fan cowl of reference 2 and to have a D-shaped inlet that transitioned to a circular shape. This new fan cowl was combined with the existing core cowl of reference 2 and was tested as an aft-mounted nacelle/pylon configuration. Data were obtained for a free-stream Mach number range from 0.70 to 0.82 over an angle-of-attack range from −3.0° to 4.0°. The design cruise conditions were a free-stream Mach number of 0.80 and a lift coefficient of 0.45.

Symbols and Abbreviations

b	wingspan, 63.121 in.
BL	buttline of model (lateral dimension), in.
c	chord measured in wing reference plane, in.
$\bar{c}$	mean geometric chord, 9.107 in.
C_D	drag coefficient, $\frac{\text{Drag}}{q_\infty S}$
ΔC_D	installed drag coefficient, $C_{D,\text{WBNP}} - C_{D,\text{WB}}$
C_L	lift coefficient, $\frac{\text{Lift}}{q_\infty S}$
C_m	pitching-moment coefficient, $\frac{\text{Pitching moment}}{q_\infty \bar{c} S}$
C_p	pressure coefficient, $(p - p_\infty)/q_\infty$
FS	fuselage station (axial dimension, positive downstream from model nose), in.
M	free-stream Mach number
NBL	nacelle buttline, in.
NS	nacelle station (axial dimension, positive downstream from nacelle lip), in.
p	local static pressure, $\frac{\text{lb}}{\text{in}^2}$
p_∞	free-stream static pressure, $\frac{\text{lb}}{\text{in}^2}$
q_∞	free-stream dynamic pressure, $\frac{\text{lb}}{\text{in}^2}$
r	core cowl radius, in.
S	wing reference area, 529.59 in^2
$t/2$	half-thickness of pylon, in.
WL	fuselage waterline, in.
WRP	wing reference plane (fig. 1(a))
x	local axial dimension, positive downstream, in.
y	local lateral dimension, positive to the right, in.
z	local vertical dimension, positive up, in.
α	angle of attack, deg
η	wing semispan location, $\frac{y}{b/2}$
ϕ	circumferential angular measurements for nacelle orifice locations (fig. 3(a)), deg

Model components:

B	body
N	nacelle
P	pylon
W	wing

Experimental Apparatus and Procedure

Wind Tunnel

The experimental investigation was conducted in the Langley 16-Foot Transonic Tunnel. This tunnel is an atmospheric, transonic, single-return tunnel with continuous air exchange and is capable of operating at Mach numbers from 0.20 to 1.30. A detailed description of the tunnel is presented in references 3 and 4.

Model and Support System

The 1/24-scale wing-body model, representative of a wide-body transport, is shown in figure 1(a) and a photograph of the complete model installed in the 16-Foot Transonic Tunnel is shown in figure 1(b). The model was mounted on a sting-supported, six-component strain-gage balance. The wing had supercritical airfoil sections and was located in a high-wing position.

Details of the fuselage, wing, and wing pressure orifice locations are given in references 1 and 5. The location of the nacelle/pylon and the rows of pressure orifices just inboard and outboard of the nacelle are shown in figure 2.

The short duct, separate-flow nacelles of the present investigation consisted of a fan cowl and a core cowl. The details of the core cowl are given in figure 3(a). The fan cowl was designed to have the same length and internal areas as the fan cowl of reference 2 and to have a D-shaped inlet that transitioned to a circular shape. The fan cowl is shown in figure 3(b). The internal and external contours of the fan cowl below WL 1.250 were semicircular. The internal contour above WL 1.250 began as a rectangular shape that faired into a semicircular shape at nacelle station 3.610 and continued as a semicircular shape to the base of the cowl (NS 6.109). The external contour above WL 1.250 was a rectangular shape up to the wing trailing edge and then faired into a semicircular shape at the base of the fan cowl. Three typical cross-sectional shapes are shown in figure 3(b). Since the fan cowl was symmetrical with respect to the x-z plane, only the coordinates for the external and internal geometry of the right-hand side of the fan (positive y direction) are given in tables I and II, respectively.

A typical section and coordinates of the fan cowl bottom centerline lip are also shown in figure 3(b). A portion of the fan cowl was cut away to match the wing lower surface contour as shown by the cross-hatched region of figure 3(b).

The diverter shown in figure 2 was the same as used in reference 2. The pylon and that part of the fan cowl extending above the wing upper surface are shown in figure 4.

Instrumentation and Data Reduction

The model aerodynamic force and moment data were obtained by an internally mounted, six-component strain-gage balance. The model static pressures were measured by eight electronically scanned pressure transducer units located in the model nose to reduce the lag time required between data points. Sting cavity pressures were measured by individual remotely located strain-gage transducers. The attitude of the model was determined by using an accelerometer-type angle-of-attack measuring device located in the model.

All wind-tunnel parameters and model data were recorded simultaneously on magnetic tape. Except for electronically scanned pressure transducer pressures, averaged values were used to compute all parameters. The model angle of attack was corrected for tunnel upflow, which was determined from inverted model runs in a previous tunnel test (ref. 5). Sting cavity pressures were used to correct the longitudinal balance components for pressure forces in the sting cavity. Since the pressures measured inside the nacelles were not different from those of reference 2, the drag data were corrected with the internal drag corrections obtained in reference 2 for the aft-mounted nacelle.

Skin-friction drag was calculated with the method of Frankl and Voishel (ref. 6) for compressible, turbulent flow over a flat plate. The forces and moments were transferred to the model moment center—the quarter-chord point of the mean geometric chord on waterline 0.0.

Tests

This experimental wind-tunnel investigation was conducted in the Langley 16-Foot Transonic Tunnel at free-stream Mach numbers from 0.70 to 0.82 and Reynolds numbers from approximately 2.5×10^6 to 3.0×10^6 based on the mean geometric chord of the wing. The model angle of attack varied from -3.0° to 4.0°. Boundary layer transition on the model was fixed with a grit transition-strip procedure (ref. 7). A 0.1-in.-wide strip of No. 100 carborundum grains was attached 1.0 in. behind the nose of the fuselage. Strips of No. 90 and No. 80 grains were applied on the upper and lower wing surfaces as shown in figure 11 of reference 1. The transition strips were located further rearward than usual in an effort to more nearly simulate the aerodynamic behavior of the wing at full-scale Reynolds numbers (ref. 8). A 0.1-in.-wide strip of No. 120 grit was placed 0.375 in. aft of the nacelle lip of the fan and core cowls on the external and internal surfaces.

Results and Discussion

The longitudinal aerodynamic characteristics are presented in figure 5 over the Mach number range. The addition of the nacelle/pylon resulted in increases in drag and lift over that of the wing-body configuration. The increase in lift associated with the addition of the nacelle/pylon is common for the aft-mounted nacelles (see refs. 1 and 2). The installed drag coefficient $(\Delta C_D = C_{D,\mathrm{WBNP}} - C_{D,\mathrm{WB}})$ is presented in figure 6 for $M = 0.80$ and $C_L = 0.45$ and is compared with the installed drag of the aft-mounted circular nacelle/pylon configuration of reference 2. The unshaded area indicates the amount of installed drag that may be attributed to the calculated nacelle/pylon skin-friction drag. The shaded area represents the combined value of form and interference drag. It should be noted that the two configurations had essentially the same installed drag, but the D-shaped nacelle had slightly less skin-friction drag, hence slightly more interference and form drag. In both configurations, the interference and form drag was considered to be excessively high. The wing chordwise pressure distributions at span stations inboard and outboard of the nacelle/pylon centerline ($\eta = 0.370$) are presented in figure 7 for $M = 0.80$ and $C_L \approx 0.43$. The data for the aft-mounted nacelle configuration of reference 2 are also shown. The installation of the circular nacelle increased the wing lower surface pressure coefficients ahead of the nacelle (i.e., reduced velocity), which increased the lift. The addition of the D-shaped nacelle further increased pressures (decreased velocity) ahead of the nacelle inlet. However, near and behind the inlet, the D-shaped nacelle produced a substantial region of supersonic flow ($C_p \leq -0.435$). The net result was an increase in interference and form drag relative to the circular nacelle of reference 2 (see fig. 6). With proper nacelle alignment, it may be possible that the region of supersonic flow could have been reduced to result in an overall reduction in drag.

Summary of Results

An experimental investigation has been conducted in the Langley 16-Foot Transonic Tunnel at free-stream Mach numbers from 0.70 to 0.82 and angles of attack from -3.0° to 4.0° to determine the integration effects of D-shaped, underwing, aft-mounted, separate-flow, flow-through nacelles on a high-wing, transonic transport configuration. The results are summarized as follows:

1. The aft-mounted nacelle/pylon produced an increase in lift over that of the wing-body configuration by pressurizing much of the wing lower surface in front of the pylon.
2. For the D-shaped nacelle, the substantial region of supersonic flow over the wing, aft of the lip of the nacelle, cancelled the reduction in drag caused by the increase in pressures ahead of the lip, to increase interference and form drag compared with a similar circular-shaped nacelle.
3. The installed drag of the D-shaped nacelle was essentially the same as that of an aft-mounted circular nacelle from a previous investigation.

NASA Langley Research Center
Hampton, VA 23665-5225
October 29, 1987

References

1. Abeyounis, William K.; and Patterson, James C., Jr.: *Effect of Underwing Aft-Mounted Nacelles on the Longitudinal Aerodynamic Characteristics of a High-Wing Transport Airplane.* NASA TP-2447, 1985.
2. Lamb, Milton; and Abeyounis, William K.: *Integration Effects of Underwing Forward- and Rearward-Mounted Separate-Flow, Flow-Through Nacelles on a High-Wing Transport.* NASA TM-87627, 1986.
3. Corson, Blake W., Jr.; Runckel, Jack F.; and Igoe, William B.: *Calibration of the Langley 16-Foot Transonic Tunnel With Test Section Air Removal.* NASA TR R-423, 1974.
4. Peddrew, Kathryn H., compiler: *A User's Guide to the Langley 16-Foot Transonic Tunnel.* NASA TM-83186, 1981.
5. Lee, Edwin E., Jr.; and Pendergraft, Odis C., Jr.: *Installation Effects of Long-Duct Pylon-Mounted Nacelles on a Twin-Jet Transport Model With Swept Supercritical Wing.* NASA TP-2457, 1985.
6. Shapiro, Ascher H.: *The Dynamics and Thermodynamics of Compressible Fluid Flow. Volume II.* Ronald Press Co., c.1954.
7. Braslow, Albert L.; Hicks, Raymond M.; and Harris, Roy V., Jr.: *Use of Grit-Type Boundary-Layer-Transition Trips on Wind-Tunnel Models.* NASA TN D-3579, 1966.
8. Blackwell, James A., Jr.: *Preliminary Study of Effects of Reynolds Number and Boundary-Layer Transition Location on Shock-Induced Separation.* NASA TN D-5003, 1969.

Table I. External Coordinates of Fan Cowl

Coordinates at NS of—																			
0.000		0.112		0.262		0.505		0.786		1.085		1.348		1.610		2.344		2.616	
y	z	y	z	y	z	y	z	y	z	y	z	y	z	y	z	y	z	y	z
0.000	2.401	0.000	2.401	0.000	2.411	0.000	2.424	0.000	2.435	0.000	2.442	0.000	2.445	0.000	2.444	0.000	2.422	0.000	2.406
.176	2.401	.174	2.401	.177	2.411	.181	2.424	.185	2.435	.187	2.442	.189	2.445	.190	2.444	.190	2.422	.189	2.406
.353	2.401	.348	2.401	.354	2.411	.362	2.424	.369	2.435	.375	2.442	.378	2.445	.380	2.444	.380	2.422	.379	2.406
.529	2.401	.523	2.401	.531	2.411	.543	2.424	.554	2.435	.562	2.442	.567	2.445	.570	2.444	.570	2.422	.568	2.406
.705	2.401	.697	2.401	.708	2.411	.725	2.424	.738	2.435	.749	2.442	.756	2.445	.760	2.444	.760	2.422	.758	2.406
.882	2.401	.871	2.401	.885	2.411	.906	2.424	.923	2.435	.936	2.442	.945	2.445	.950	2.444	.950	2.422	.947	2.406
1.058	2.401	1.045	2.401	1.063	2.411	1.087	2.424	1.107	2.435	1.124	2.442	1.134	2.445	1.140	2.444	1.140	2.422	1.136	2.406
1.234	2.401	1.219	2.401	1.240	2.411	1.268	2.424	1.292	2.435	1.311	2.442	1.326	2.445	1.330	2.444	1.330	2.422	1.326	2.406
1.410	2.401	1.393	2.401	1.417	2.411	1.449	2.424	1.477	2.435	1.498	2.442	1.512	2.445	1.520	2.444	1.520	2.422	1.515	2.406
1.587	2.401	1.568	2.401	1.594	2.411	1.630	2.424	1.661	2.435	1.685	2.442	1.700	2.445	1.710	2.444	1.710	2.420	1.705	2.403
1.763	2.401	1.742	2.401	1.771	2.411	1.811	2.424	1.846	2.435	1.873	2.442	1.889	2.444	1.900	2.442	1.900	2.410	1.893	2.387
1.763	2.236	1.884	2.343	1.936	2.377	1.989	2.399	2.028	2.412	2.057	2.415	2.074	2.411	2.082	2.400	2.070	2.336	2.059	2.303
1.763	2.070	1.886	2.167	1.946	2.198	2.010	2.221	2.061	2.234	2.098	2.238	2.120	2.233	2.132	2.221	2.127	2.157	2.120	2.126
1.763	1.905	1.886	1.992	1.946	2.021	2.010	2.040	2.061	2.050	2.099	2.050	2.122	2.044	2.135	2.031	2.135	1.967	2.132	1.937
1.763	1.739	1.886	1.818	1.946	1.844	2.010	1.859	2.061	1.865	2.099	1.863	2.122	1.855	2.135	1.841	2.137	1.777	2.135	1.748
1.763	1.574	1.886	1.644	1.946	1.667	2.010	1.678	2.061	1.681	2.099	1.676	2.122	1.666	2.135	1.651	2.137	1.587	2.135	1.558
1.763	1.408	1.886	1.469	1.946	1.490	2.010	1.497	2.061	1.496	2.099	1.489	2.122	1.477	2.135	1.461	2.137	1.397	2.135	1.369
1.763	1.243	1.886	1.295	1.946	1.312	2.010	1.315	2.061	1.311	2.099	1.301	2.122	1.288	2.135	1.271	2.137	1.207	2.135	1.179
1.763	1.077	1.886	1.121	1.946	1.135	2.010	1.134	2.061	1.127	2.099	1.114	2.122	1.099	2.135	1.081	2.137	1.017	2.135	.990
1.763	.912	1.886	.947	1.946	.958	2.010	.953	2.061	.942	2.099	.927	2.122	.910	2.135	.891	2.137	.827	2.135	.801
1.763	.746	1.886	.773	1.946	.781	2.010	.772	2.061	.758	2.099	.739	2.122	.721	2.135	.701	2.137	.637	2.135	.611
1.763	.581	1.886	.598	1.946	.604	2.010	.591	2.061	.573	2.099	.552	2.122	.532	2.135	.511	2.137	.447	2.135	.422
1.763	.415	1.886	.424	1.946	.427	2.010	.410	2.061	.388	2.099	.365	2.122	.343	2.135	.321	2.137	.257	2.135	.232
1.763	.250	1.886	.250	1.946	.250	2.010	.229	2.061	.204	2.099	.178	2.122	.155	2.135	.132	2.137	.067	2.135	.043
1.718	−.142	1.839	−.170	1.930	.000	1.997	.000	2.051	.000	2.092	.000	2.116	.000	2.131	.000	2.136	.000	2.135	.000
1.588	−.514	1.699	−.568	1.815	−.452	1.884	−.474	1.940	−.492	1.984	−.507	2.012	−.518	2.031	−.526	2.049	−.540	2.053	−.544
1.391	−.860	1.475	−.926	1.596	−.862	1.660	−.906	1.713	−.942	1.756	−.973	1.784	−.994	1.803	−1.011	1.828	−1.040	1.835	−1.049
1.110	−1.142	1.176	−1.225	1.285	−1.212	1.338	−1.272	1.384	−1.324	1.420	−1.368	1.445	−1.399	1.462	−1.424	1.487	−1.468	1.495	−1.482
.765	−1.338	.818	−1.449	.900	−1.476	.938	−1.549	.971	−1.614	.998	−1.669	1.016	−1.708	1.029	−1.739	1.049	−1.795	1.055	−1.813
.392	−1.468	.419	−1.589	.463	−1.640	.483	−1.723	.501	−1.796	.515	−1.857	.524	−1.901	.531	−1.936	.542	−2.000	.546	−2.021
.000	−1.513	.000	−1.636	.000	−1.696	.000	−1.781	.000	−1.857	.000	−1.921	.000	−1.957	.000	−2.003	.000	−2.070	.000	−2.092

Table I. Concluded

Coordinates at NS of—																	
2.917		3.292		3.630		3.968		4.344		4.644		4.832		5.020		6.109	
y	z	y	z	y	z	y	z	y	z	y	z	y	z	y	z	y	z
0.000	2.384	0.000	2.350	0.000	2.314	0.000	2.272	0.000	2.217	0.000	2.167	0.000	2.133	0.000	2.096	0.000	1.831
.188	2.384	.185	2.350	.182	2.314	.177	2.272	.170	2.217	.164	2.167	.160	2.133	.156	2.096	.125	1.827
.377	2.384	.371	2.350	.363	2.314	.354	2.272	.341	2.217	.329	2.167	.320	2.133	.311	2.096	.249	1.814
.565	2.384	.556	2.350	.545	2.314	.530	2.272	.511	2.217	.493	2.167	.481	2.132	.467	2.094	.372	1.793
.753	2.384	.742	2.350	.726	2.314	.707	2.272	.682	2.217	.657	2.165	.641	2.130	.622	2.090	.494	1.763
.941	2.384	.927	2.350	.908	2.314	.884	2.272	.852	2.215	.822	2.162	.801	2.124	.778	2.082	.613	1.725
1.130	2.384	1.113	2.350	1.089	2.314	1.061	2.270	1.022	2.211	.986	2.155	.961	2.114	.933	2.068	.729	1.679
1.318	2.384	1.298	2.350	1.271	2.312	1.238	2.266	1.193	2.203	1.150	2.141	1.120	2.095	1.087	2.044	.842	1.626
1.506	2.383	1.483	2.347	1.452	2.306	1.414	2.256	1.362	2.185	1.312	2.115	1.277	2.064	1.238	2.008	.951	1.564
1.694	2.378	1.669	2.336	1.633	2.290	1.589	2.232	1.529	2.151	1.471	2.072	1.429	2.016	1.384	1.955	1.056	1.496
1.881	2.354	1.851	2.302	1.809	2.247	1.758	2.180	1.688	2.090	1.620	2.004	1.573	1.945	1.521	1.881	1.155	1.420
2.041	2.260	2.005	2.204	1.960	2.148	1.903	2.081	1.826	1.991	1.751	1.906	1.700	1.848	1.643	1.784	1.250	1.338
2.108	2.086	2.084	2.037	2.049	1.991	2.001	1.934	1.928	1.855	1.855	1.779	1.803	1.726	1.745	1.667	1.338	1.250
2.126	1.899	2.112	1.854	2.089	1.815	2.053	1.766	1.993	1.698	1.928	1.632	1.880	1.586	1.825	1.534	1.420	1.155
2.131	1.711	2.121	1.669	2.106	1.634	2.079	1.591	2.031	1.532	1.976	1.475	1.934	1.435	1.885	1.390	1.496	1.056
2.132	1.523	2.124	1.484	2.112	1.452	2.091	1.414	2.053	1.363	2.006	1.313	1.971	1.279	1.927	1.241	1.564	.951
2.132	1.334	2.125	1.298	2.114	1.271	2.096	1.238	2.064	1.193	2.024	1.150	1.994	1.120	1.955	1.088	1.626	.842
2.132	1.146	2.125	1.113	2.115	1.089	2.098	1.061	2.069	1.022	2.034	.986	2.007	.961	1.974	.933	1.679	.729
2.132	.958	2.125	.927	2.115	.908	2.099	.884	2.071	.852	2.039	.822	2.015	.801	1.985	.778	1.725	.613
2.132	.770	2.125	.742	2.115	.726	2.099	.707	2.072	.682	2.042	.657	2.019	.641	1.992	.622	1.763	.494
2.132	.581	2.125	.556	2.115	.545	2.099	.530	2.073	.511	2.043	.493	2.021	.481	1.995	.467	1.793	.372
2.132	.393	2.125	.371	2.115	.363	2.099	.354	2.073	.341	2.043	.329	2.021	.320	1.996	.311	1.814	.249
2.132	.205	2.125	.185	2.115	.182	2.099	.177	2.073	.170	2.043	.164	2.022	.160	1.996	.156	1.827	.125
2.132	.016	2.125	.000	2.115	.000	2.099	.000	2.073	.000	2.043	.000	2.022	.000	1.996	.000	1.831	.000
2.132	.000	2.053	-.550	2.043	-.547	2.028	-.543	2.002	-.536	1.973	-.529	1.953	-.523	1.928	-.517	1.768	-.474
2.056	-.549	1.840	-1.063	1.832	-1.058	1.818	-1.050	1.795	-1.036	1.769	-1.022	1.751	-1.011	1.729	-.998	1.586	-.915
1.841	-1.059	1.503	-1.503	1.496	-1.496	1.484	-1.484	1.466	-1.466	1.445	-1.445	1.429	-1.429	1.411	-1.411	1.295	-1.295
1.502	-1.497	1.063	-1.840	1.058	-1.832	1.050	-1.818	1.036	-1.795	1.022	-1.769	1.011	-1.751	.998	-1.729	.915	-1.586
1.061	-1.833	.550	-2.053	.547	-2.043	.543	-2.028	.536	-2.002	.529	-1.973	.523	-1.953	.517	-1.928	.474	-1.768
.549	-2.044	.000	-2.125	.000	-2.115	.000	-2.099	.000	-2.073	.000	-2.043	.000	-2.022	.000	-1.996	.000	-1.831
.000	-2.116																

Table II. Internal Coordinates of Fan Cowl

Coordinates at NS of—																			
0.000		0.397		0.547		0.697		0.847		1.146		1.446		1.745		2.045		2.344	
y	z	y	z	y	z	y	z	y	z	y	z	y	z	y	z	y	z	y	z
0.000	1.642	0.000	1.496	0.000	1.500	0.000	1.508	0.000	1.519	0.000	1.547	0.000	1.582	0.000	1.620	0.000	1.656	0.000	1.686
.353	1.642	.251	1.496	.252	1.500	.255	1.507	.259	1.516	.270	1.543	.284	1.575	.298	1.610	.312	1.643	.325	1.669
.705	1.642	.502	1.496	.504	1.497	.510	1.502	.518	1.509	.540	1.529	.567	1.554	.595	1.580	.622	1.602	.647	1.616
1.058	1.642	.754	1.496	.757	1.493	.765	1.493	.777	1.495	.809	1.503	.847	1.514	.887	1.524	.926	1.528	.958	1.522
1.410	1.642	1.005	1.496	1.009	1.485	1.019	1.477	1.035	1.471	1.076	1.460	1.123	1.448	1.171	1.432	1.215	1.409	1.249	1.376
1.763	1.642	1.256	1.496	1.261	1.472	1.273	1.449	1.290	1.428	1.334	1.383	1.383	1.335	1.429	1.283	1.467	1.226	1.494	1.163
1.763	1.364	1.507	1.496	1.510	1.434	1.516	1.377	1.525	1.323	1.550	1.225	1.580	1.135	1.612	1.050	1.639	.966	1.658	.882
1.763	1.085	1.533	1.087	1.529	1.135	1.538	1.089	1.545	1.046	1.570	.967	1.601	.894	1.633	.824	1.661	.755	1.680	.686
1.763	.807	1.547	.873	1.549	.836	1.556	.802	1.565	.769	1.591	.709	1.622	.652	1.654	.597	1.682	.544	1.702	.490
1.763	.528	1.560	.665	1.569	.537	1.576	.514	1.585	.492	1.611	.450	1.643	.410	1.675	.371	1.704	.333	1.724	.294
1.763	.250	1.587	.250	1.589	.238	1.596	.227	1.605	.215	1.631	.192	1.663	.168	1.696	.145	1.725	.122	1.746	.098
1.718	−.142	1.547	−.103	1.571	.000	1.579	.000	1.590	.000	1.620	.000	1.655	.000	1.690	.000	1.721	.000	1.743	.000
1.588	−.515	1.429	−.438	1.491	−.312	1.501	−.315	1.513	−.320	1.546	−.330	1.583	−.341	1.622	−.353	1.656	−.363	1.681	−.372
1.379	−.850	1.240	−.739	1.349	−.601	1.360	−.608	1.373	−.617	1.405	−.637	1.442	−.660	1.481	−.683	1.515	−.704	1.541	−.722
1.100	−1.129	.989	−.990	1.153	−.855	1.162	−.866	1.174	−.879	1.204	−.909	1.238	−.942	1.273	−.976	1.304	−1.007	1.329	−1.033
.765	−1.339	.688	−1.179	.909	−1.065	.917	−1.079	.927	−1.095	.952	−1.134	.980	−1.176	1.008	−1.219	1.034	−1.259	1.055	−1.292
.392	−1.469	.353	−1.297	.627	−1.222	.633	−1.238	.640	−1.257	.658	−1.301	.678	−1.350	.698	−1.401	.717	−1.447	.732	−1.486
.000	−1.513	.000	−1.337	.320	−1.318	.323	−1.336	.327	−1.356	.336	−1.405	.347	−1.458	.357	−1.513	.367	−1.564	.375	−1.606
				.000	−1.351	.000	−1.369	.000	−1.390	.000	−1.439	.000	−1.495	.000	−1.551	.000	−1.603	.000	−1.648

Table II. Concluded

Coordinates at NS of—																			
2.644		3.015		3.610		3.981		4.279		4.725		5.171		5.358		5.508		6.109	
y	z	y	z	y	z	y	z	y	z	y	z	y	z	y	z	y	z	y	z
0.000	1.705	0.000	1.723	0.000	1.764	0.000	1.778	0.000	1.794	0.000	1.823	0.000	1.861	0.000	1.877	0.000	1.877	0.000	1.818
.336	1.684	.347	1.696	.545	1.677	.549	1.691	.554	1.706	.563	1.734	.575	1.770	.580	1.785	.580	1.785	.562	1.729
.666	1.619	.685	1.614	1.037	1.427	1.045	1.439	1.054	1.451	1.072	1.475	1.094	1.506	1.103	1.519	1.103	1.519	1.069	1.471
.982	1.504	1.003	1.473	1.427	1.037	1.439	1.045	1.451	1.054	1.475	1.072	1.506	1.094	1.519	1.103	1.519	1.103	1.471	1.069
1.270	1.332	1.286	1.271	1.677	.545	1.691	.549	1.706	.554	1.734	.563	1.770	.575	1.785	.580	1.785	.580	1.729	.562
1.507	1.094	1.513	1.008	1.764	.000	1.778	.000	1.794	.000	1.823	.000	1.861	.000	1.877	.000	1.877	.000	1.818	.000
1.665	.798	1.666	.696	1.677	−.545	1.691	−.549	1.706	−.554	1.734	−.563	1.770	−.575	1.785	−.580	1.785	−.580	1.729	−.562
1.687	.617	1.688	.533	1.427	−1.037	1.439	−1.045	1.431	−1.054	1.475	−1.072	1.506	−1.094	1.519	−1.103	1.519	−1.103	1.471	−1.069
1.709	.436	1.710	.371	1.037	−1.427	1.045	−1.439	1.054	−1.451	1.072	−1.475	1.094	−1.506	1.103	−1.519	1.103	−1.519	1.069	−1.471
1.731	.256	1.732	.209	.545	−1.677	.549	−1.691	.554	−1.706	.563	−1.734	.575	−1.770	.580	−1.785	.580	−1.785	.562	−1.729
1.753	.075	1.754	.046	.000	−1.764	.000	−1.778	.000	−1.794	.000	−1.823	.000	−1.861	.000	−1.877	.000	−1.877	.000	1.818
1.752	.000	1.753	.000																
1.694	−.378	1.701	−.383																
1.555	−.734	1.566	−.744																
1.343	−1.051	1.355	−1.068																
1.068	−1.315	1.078	−1.337																
.741	−1.514	.749	−1.540																
.380	−1.637	.384	−1.665																
.000	−1.678	.000	−1.708																

Wing details

Aspect ratio	7.523
Taper ratio	0.328
Area (trapezoid)	529.590
$\bar{c}$	9.107
Incidence	0°
Dihedral	0°

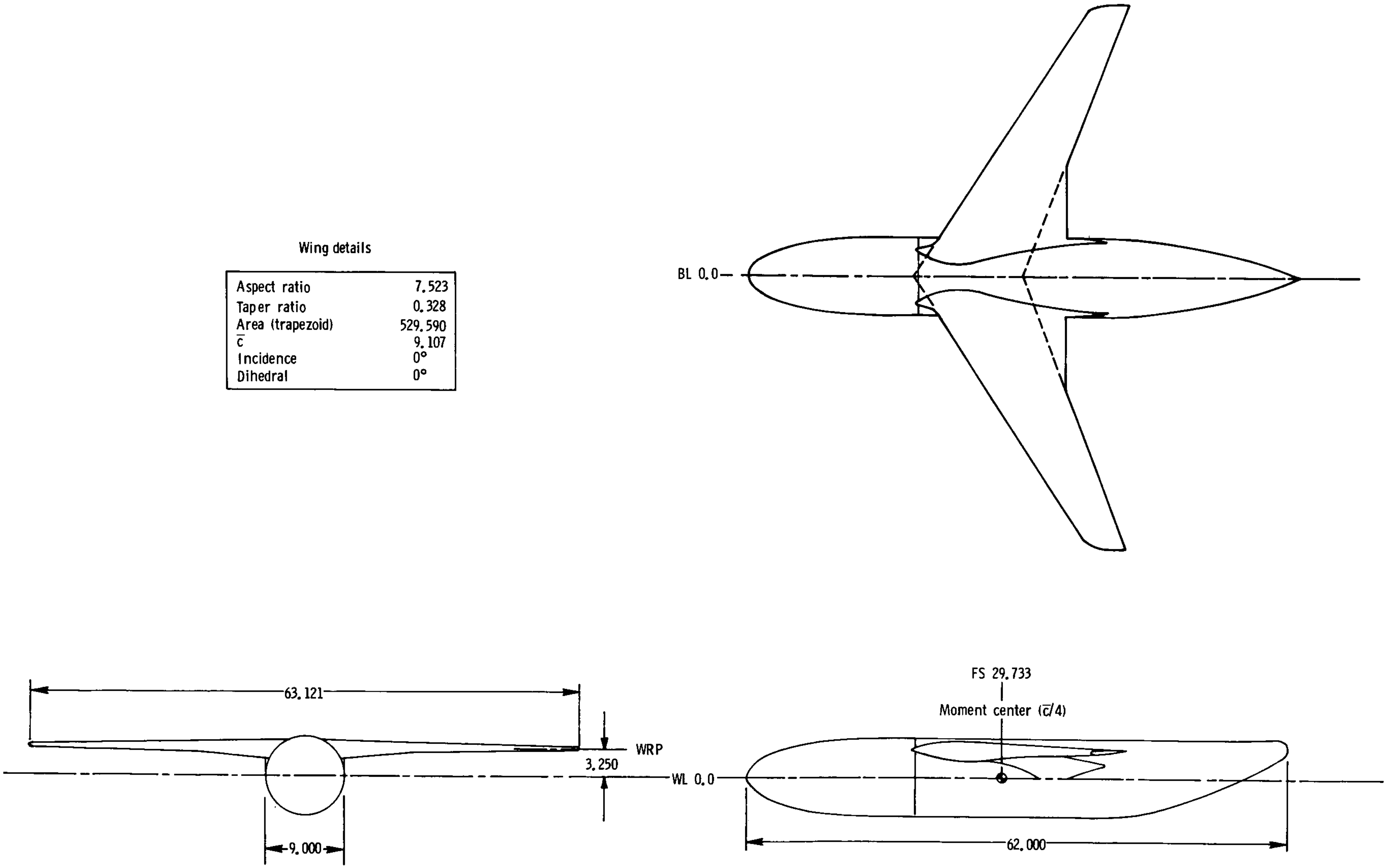

(a) General layout.

Figure 1. Details of wing-body model. All linear dimensions are in inches.

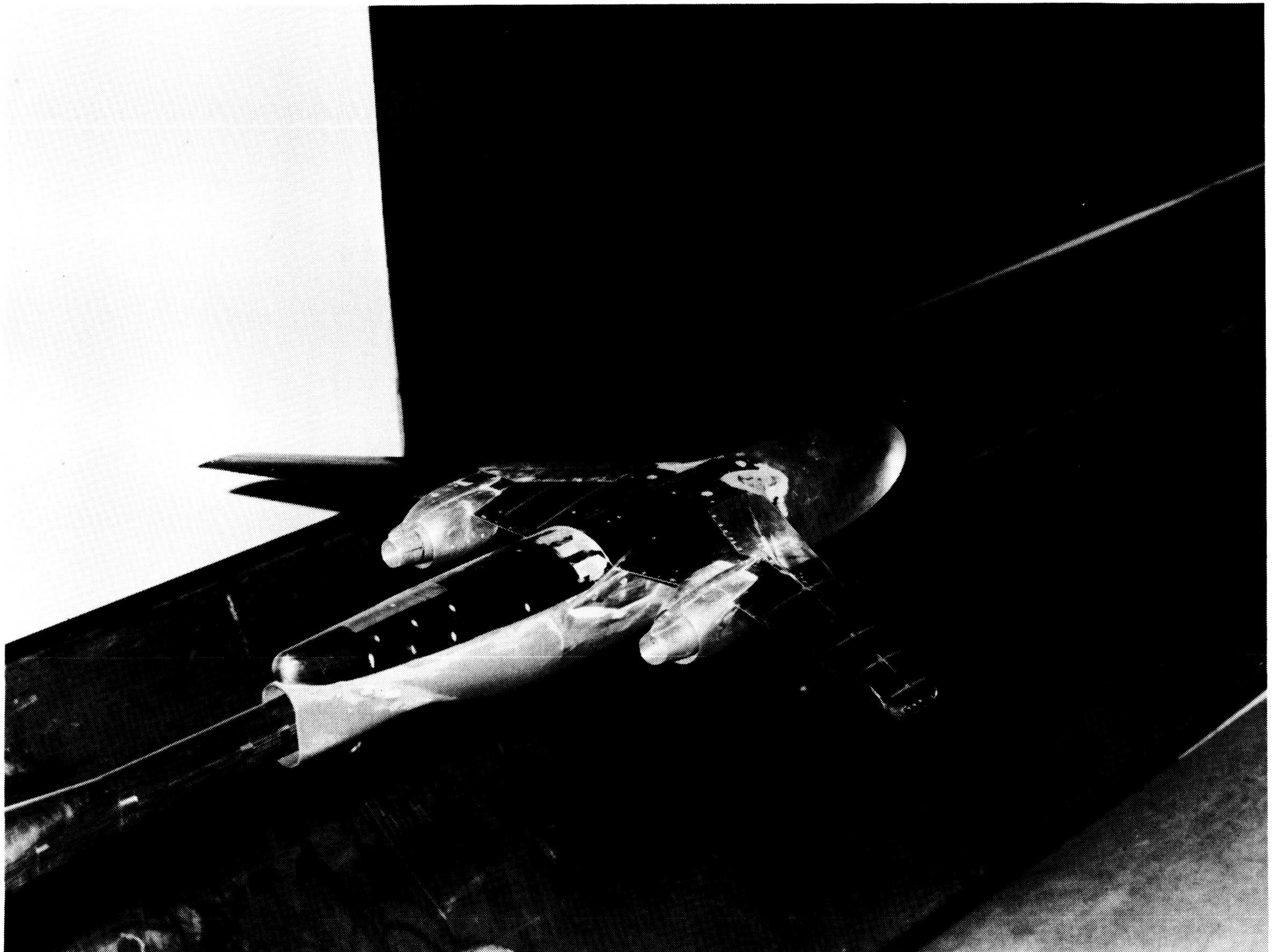

L-86-9767

(b) Model installed in the Langley 16-Foot Transonic Tunnel.

Figure 1. Concluded.

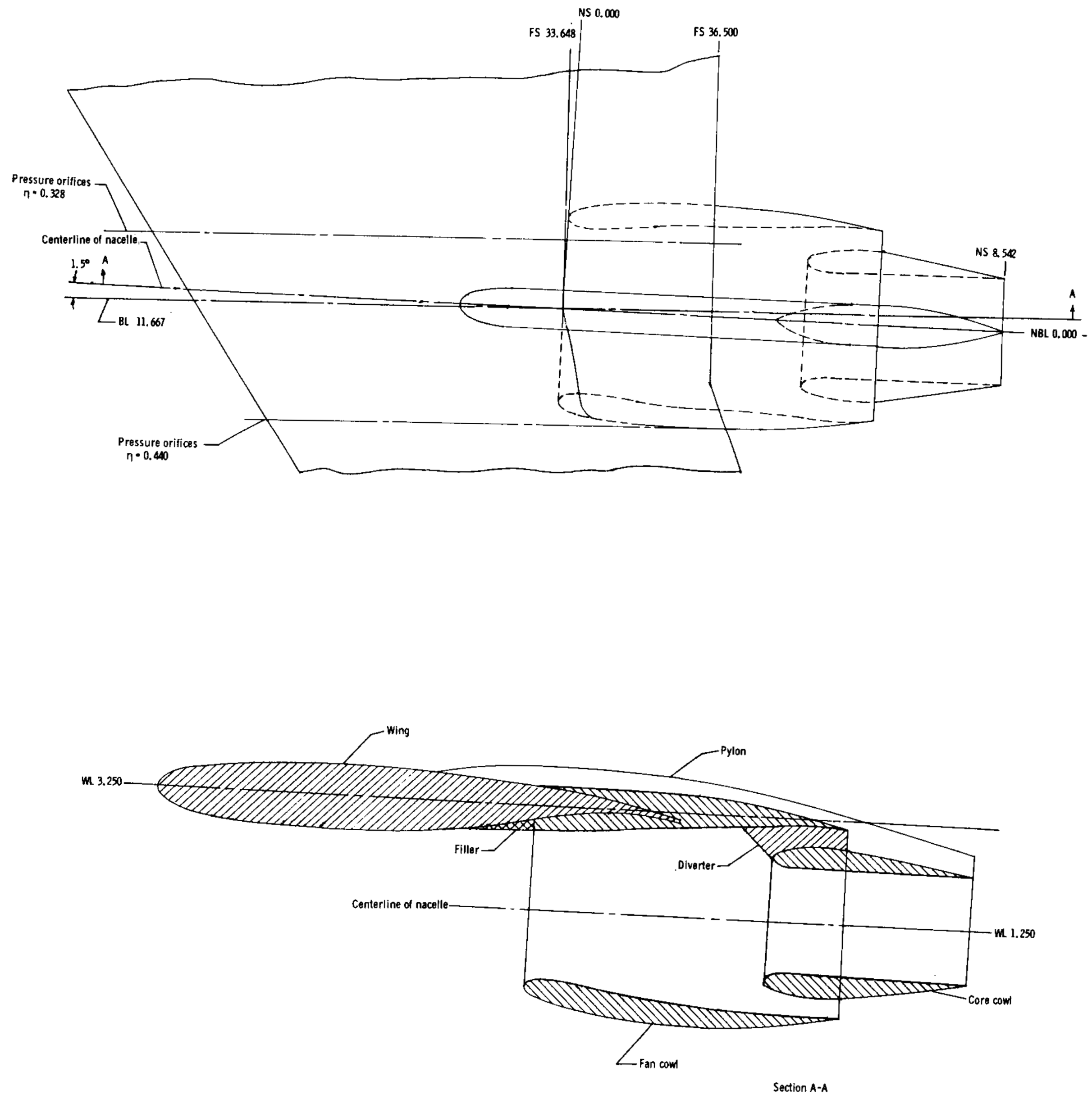

Figure 2. Nacelle/pylon location. Linear dimensions are in inches.

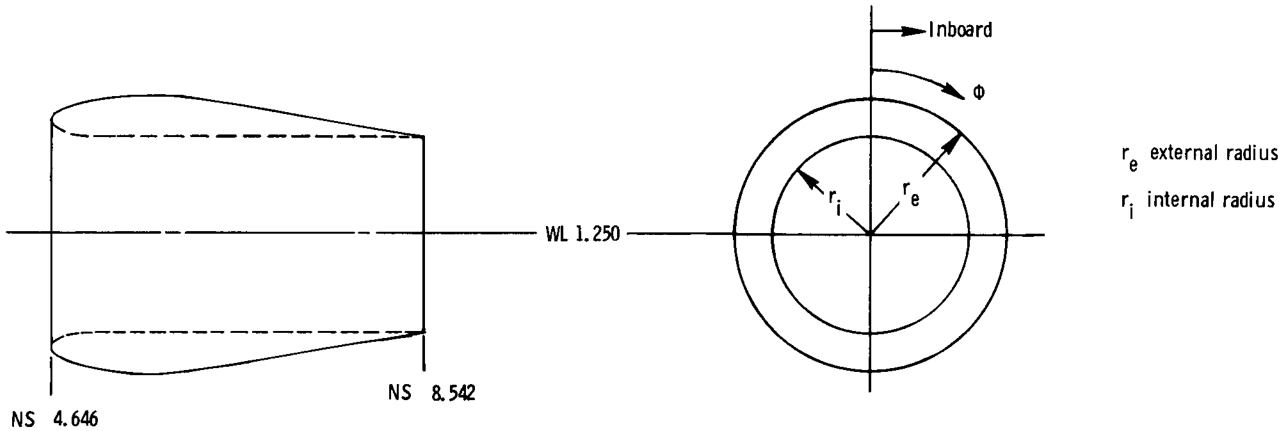

External contour			
NS	r	NS	r
4.646	1.168	5.229	1.398
4.648	1.184	5.273	1.404
4.668	1.218	5.318	1.410
4.685	1.233	5.363	1.415
4.702	1.246	5.408	1.419
4.736	1.266	5.453	1.423
4.747	1.272	5.497	1.427
4.769	1.283	5.542	1.429
4.803	1.297	5.587	1.434
4.825	1.305	5.632	1.434
4.870	1.320	5.676	1.435
4.915	1.334	5.744	1.436
4.949	1.343	5.771	1.437
5.005	1.357	5.846	1.433
5.083	1.373	5.884	1.430
5.139	1.384	5.921	1.426
5.184	1.391	5.949	1.421
5.206	1.394	8.542	0.996

Internal contour	
NS	r
4.646	1.168
4.649	1.147
4.655	1.134
4.663	1.120
4.674	1.107
4.695	1.088
4.723	1.070
4.755	1.054
4.792	1.039
4.833	1.026
4.877	1.015
4.941	1.004
4.991	0.999
5.043	0.996
5.078	0.996
8.542	0.996

NS	External pressure orifices at Φ of		
	30°	90°	180°
6.034	↓	↓	↓
6.785	↓	↓	↓
7.461	↓	↓	↓
8.174	↓	↓	↓

Internal pressure orifices located at NS 6.409 for Φ of 0°, 90°, 180° and 270°

(a) Core cowl.

Figure 3. Details of nacelles. Linear dimensions are in inches.

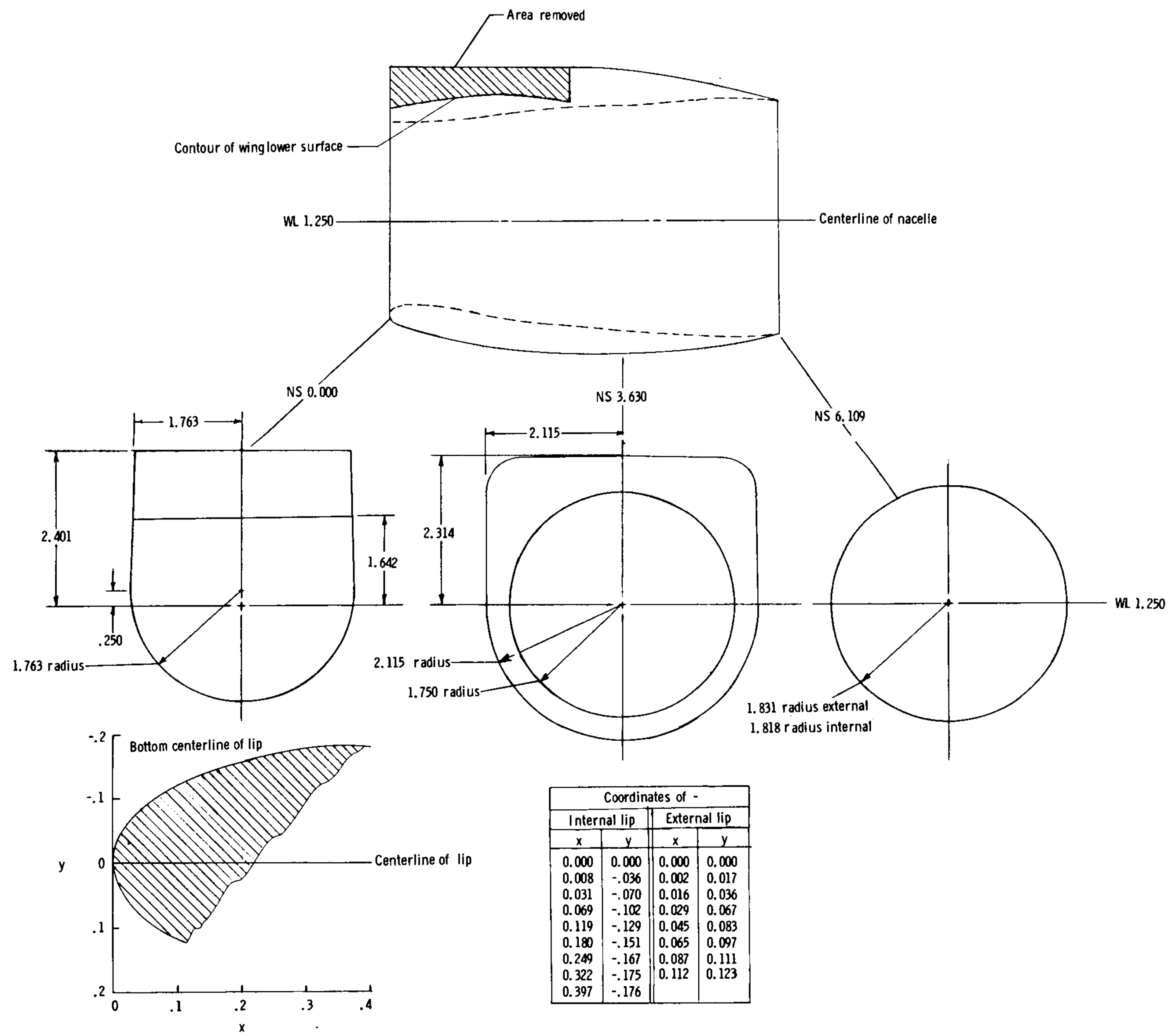

Coordinates of -			
Internal lip		External lip	
x	y	x	y
0.000	0.000	0.000	0.000
0.008	-.036	0.002	0.017
0.031	-.070	0.016	0.036
0.069	-.102	0.029	0.067
0.119	-.129	0.045	0.083
0.180	-.151	0.065	0.097
0.249	-.167	0.087	0.111
0.322	-.175	0.112	0.123
0.397	-.176		

(b) Basic fan cowl.

Figure 3. Concluded.

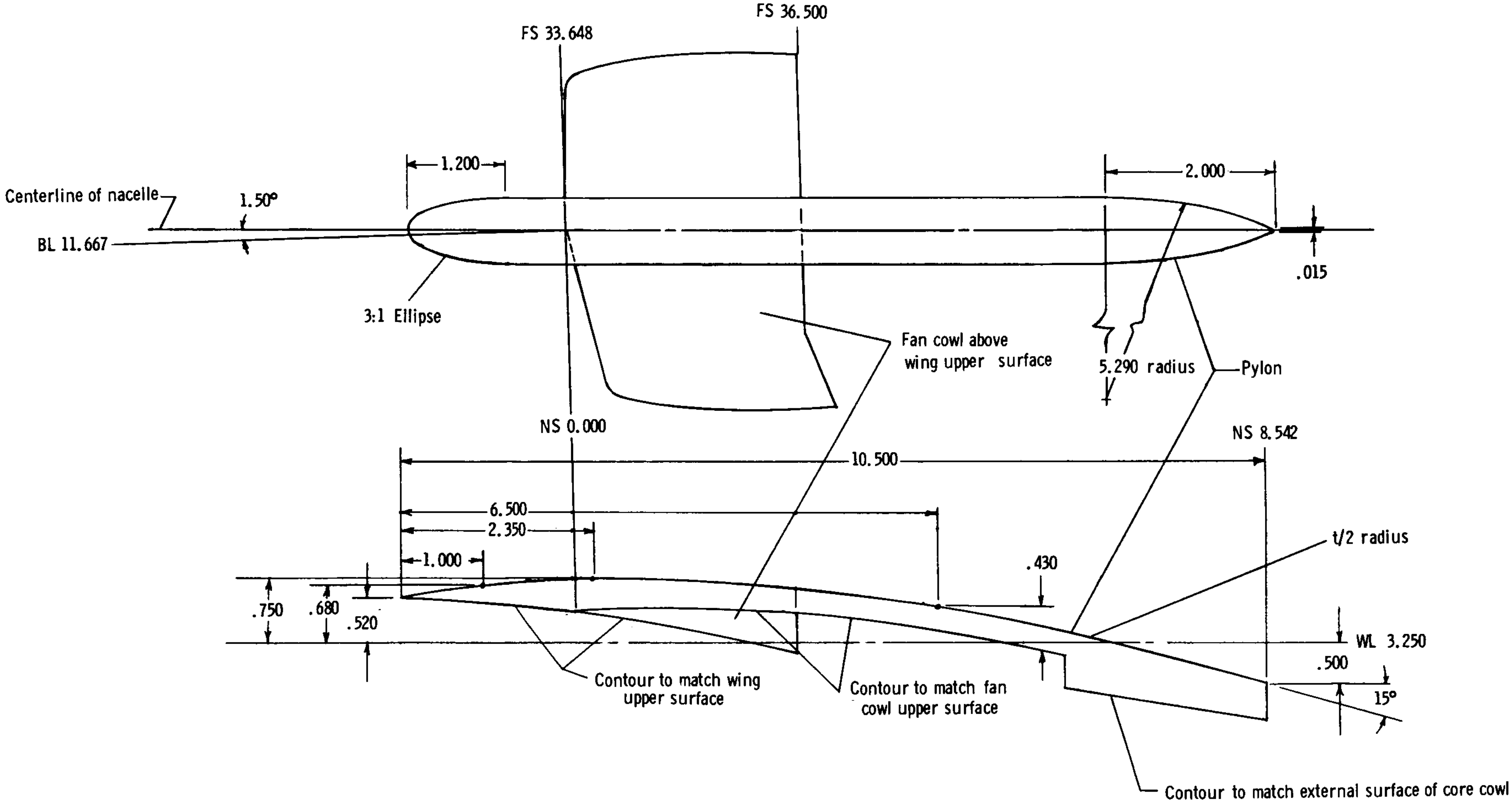

Figure 4. Details of pylon. Linear dimensions are in inches.

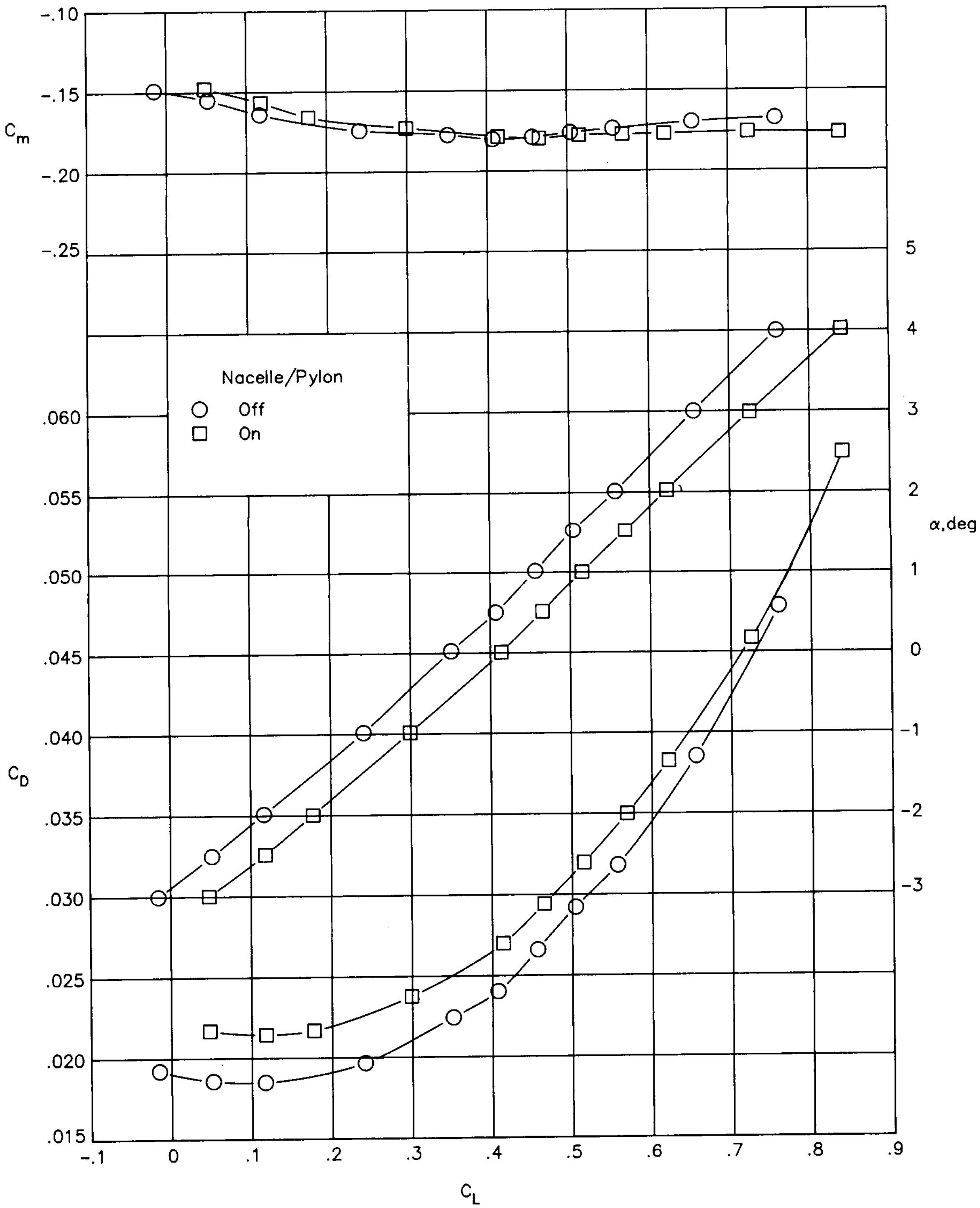

(a) $M = 0.70$.

Figure 5. Effect of nacelle/pylon on longitudinal aerodynamics characteristics.

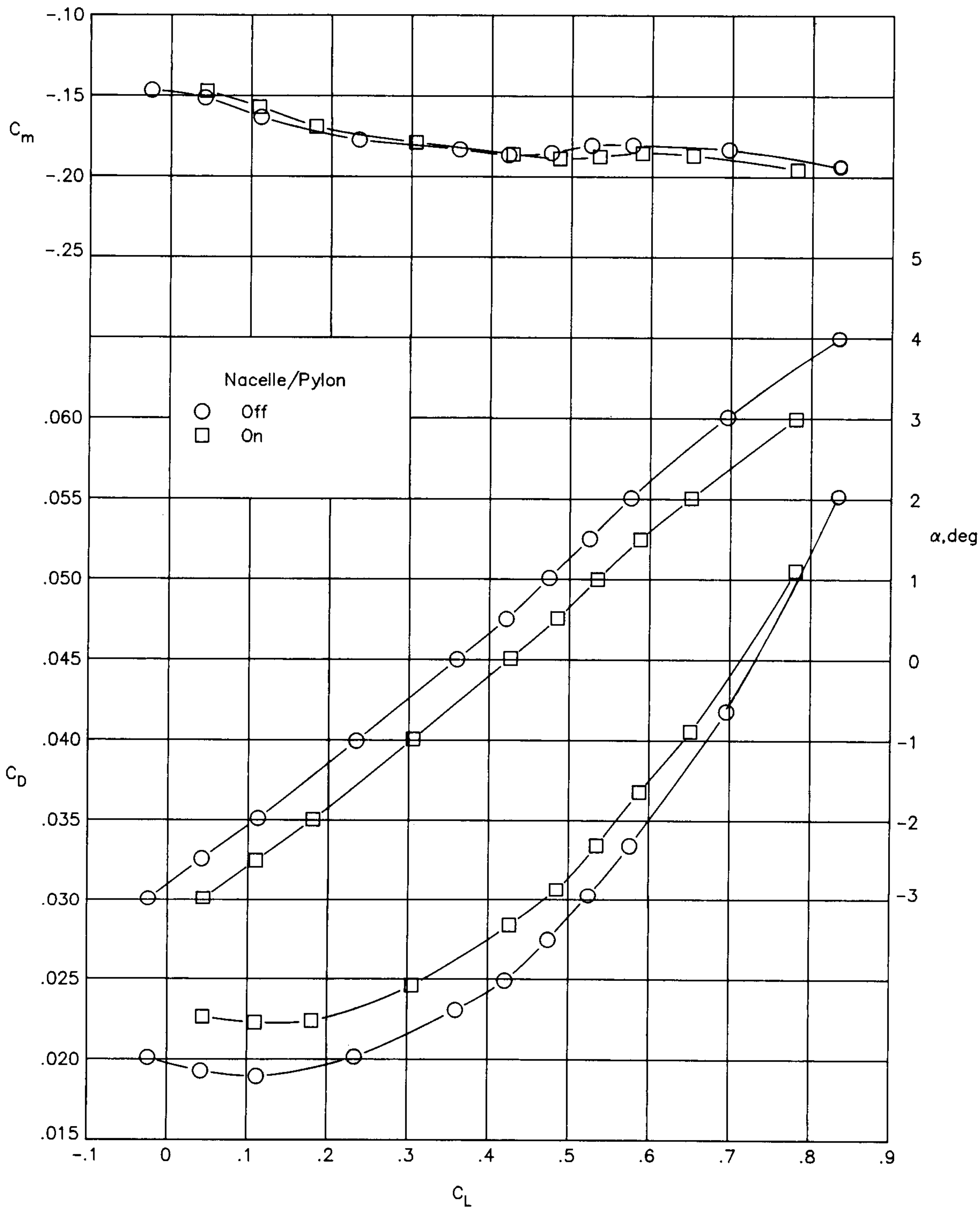

(b) $M = 0.75$.

Figure 5. Continued.

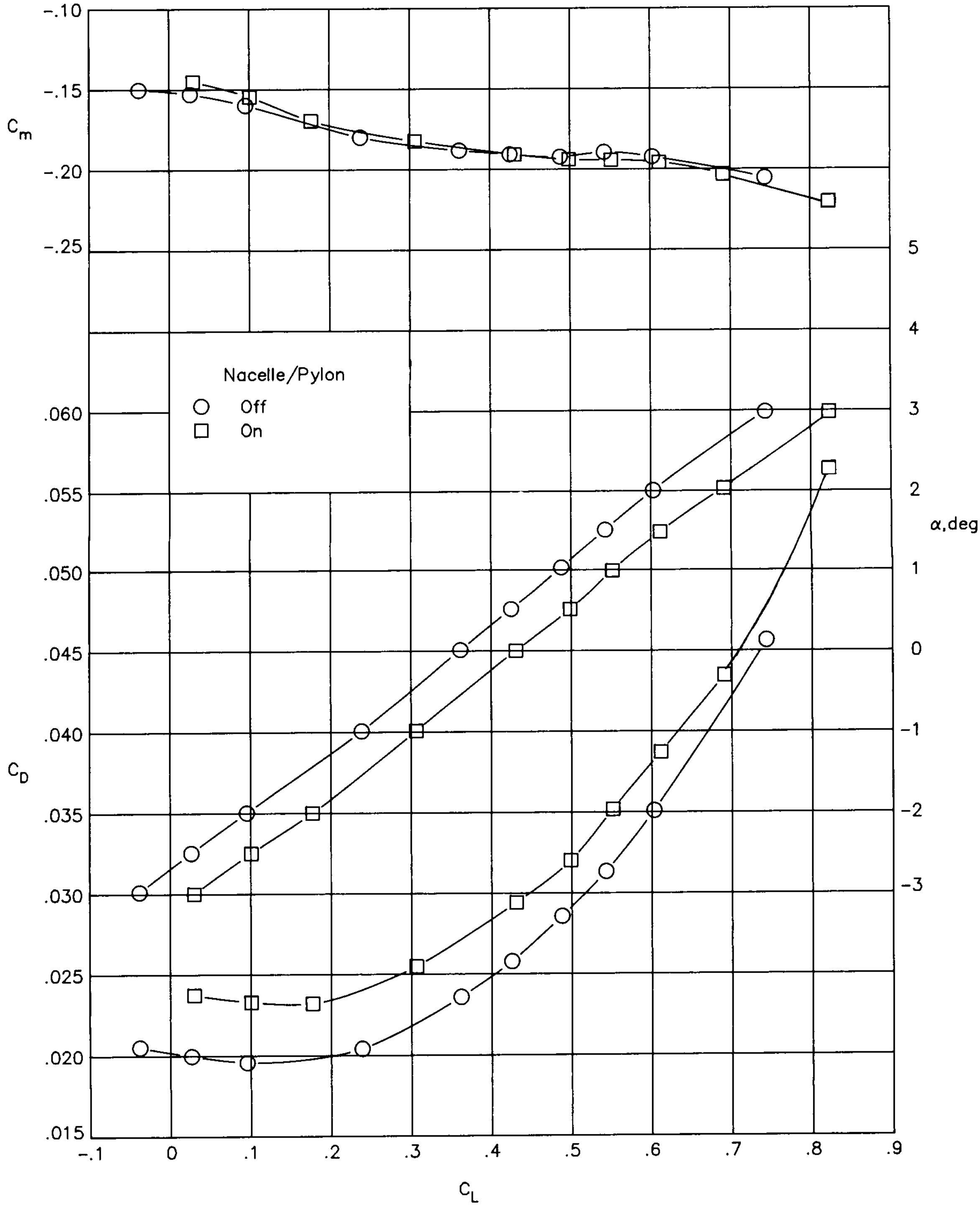

(c) $M = 0.78$.

Figure 5. Continued.

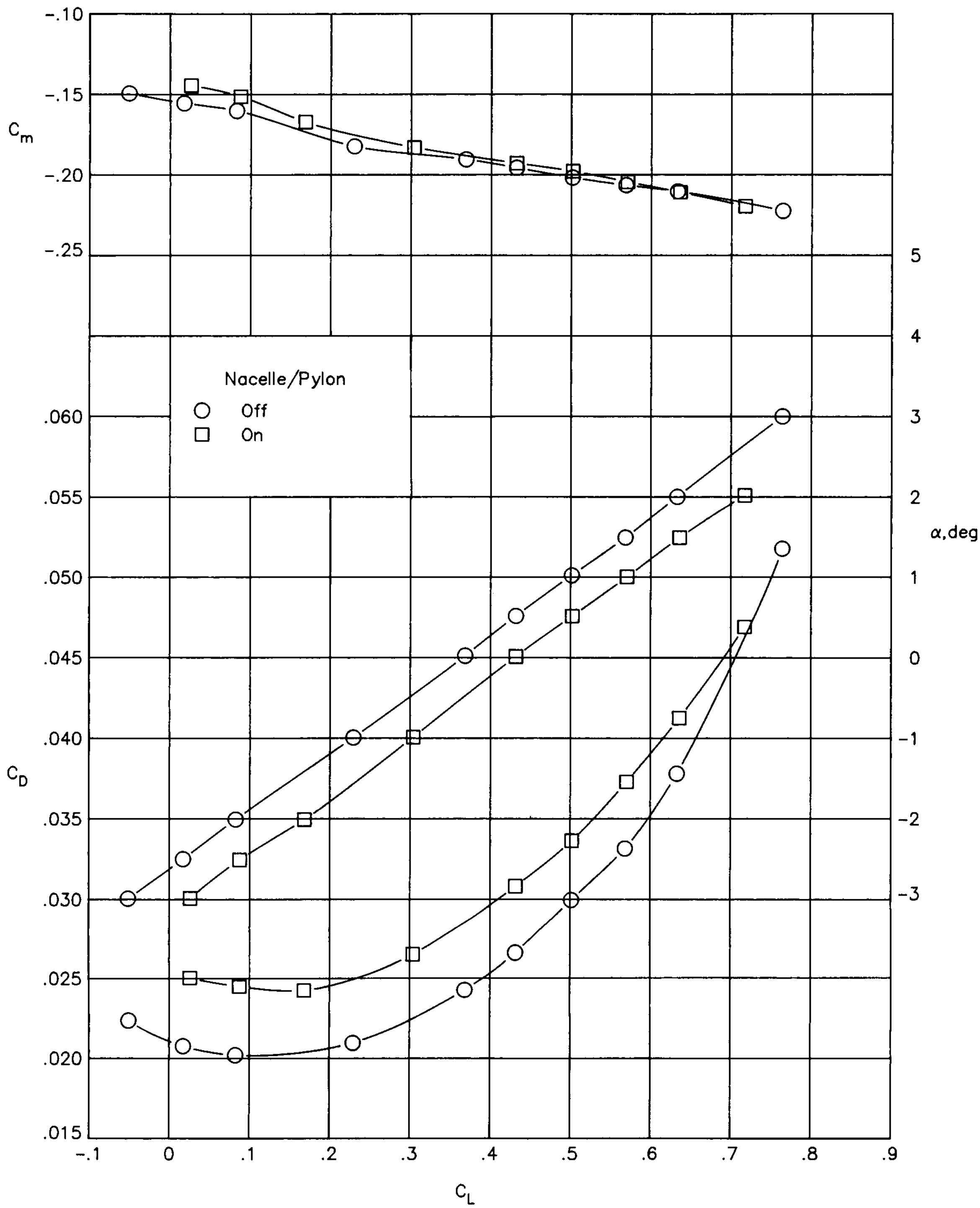

(d) $M = 0.80$.

Figure 5. Continued.

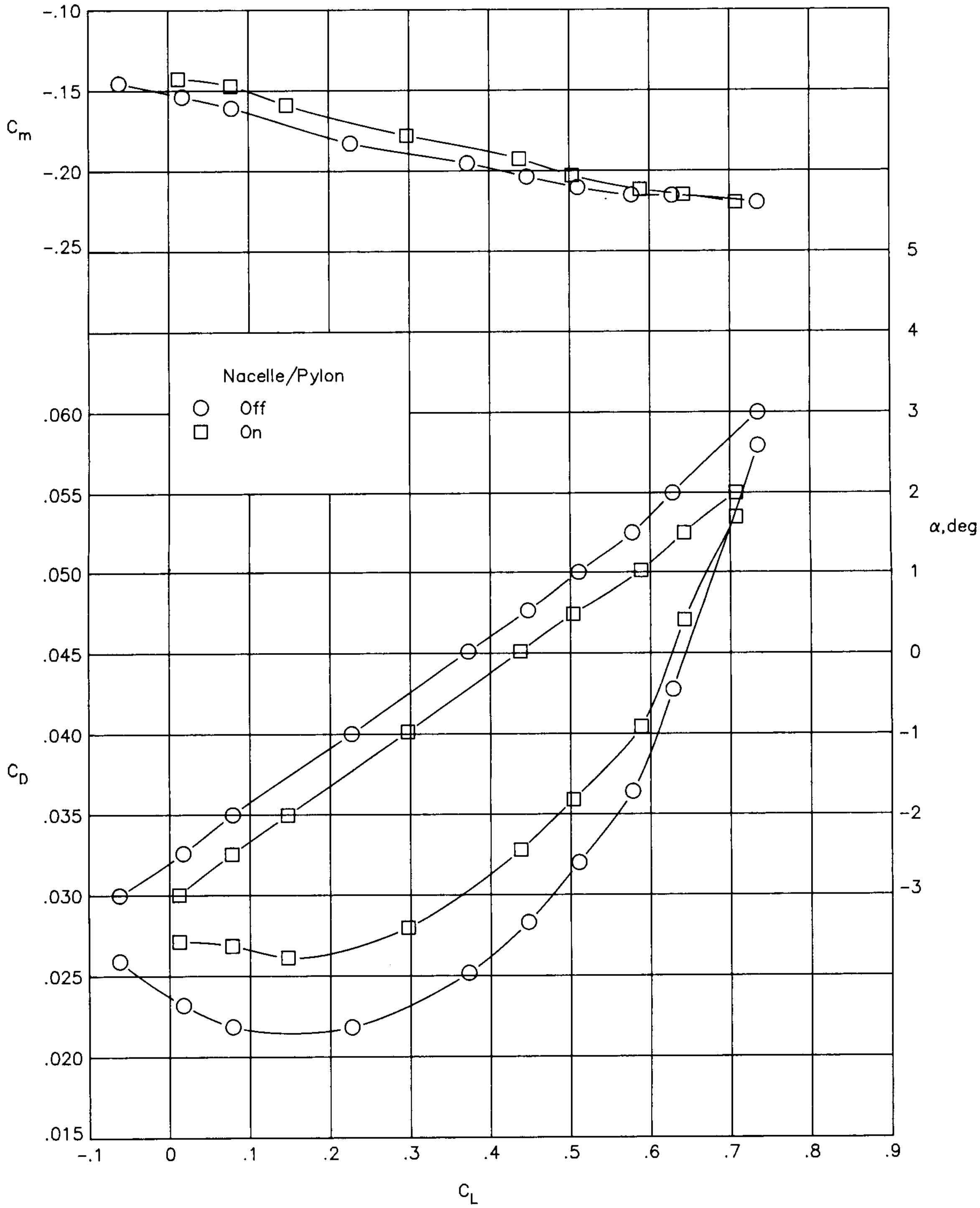

(e) $M = 0.82$.

Figure 5. Concluded.

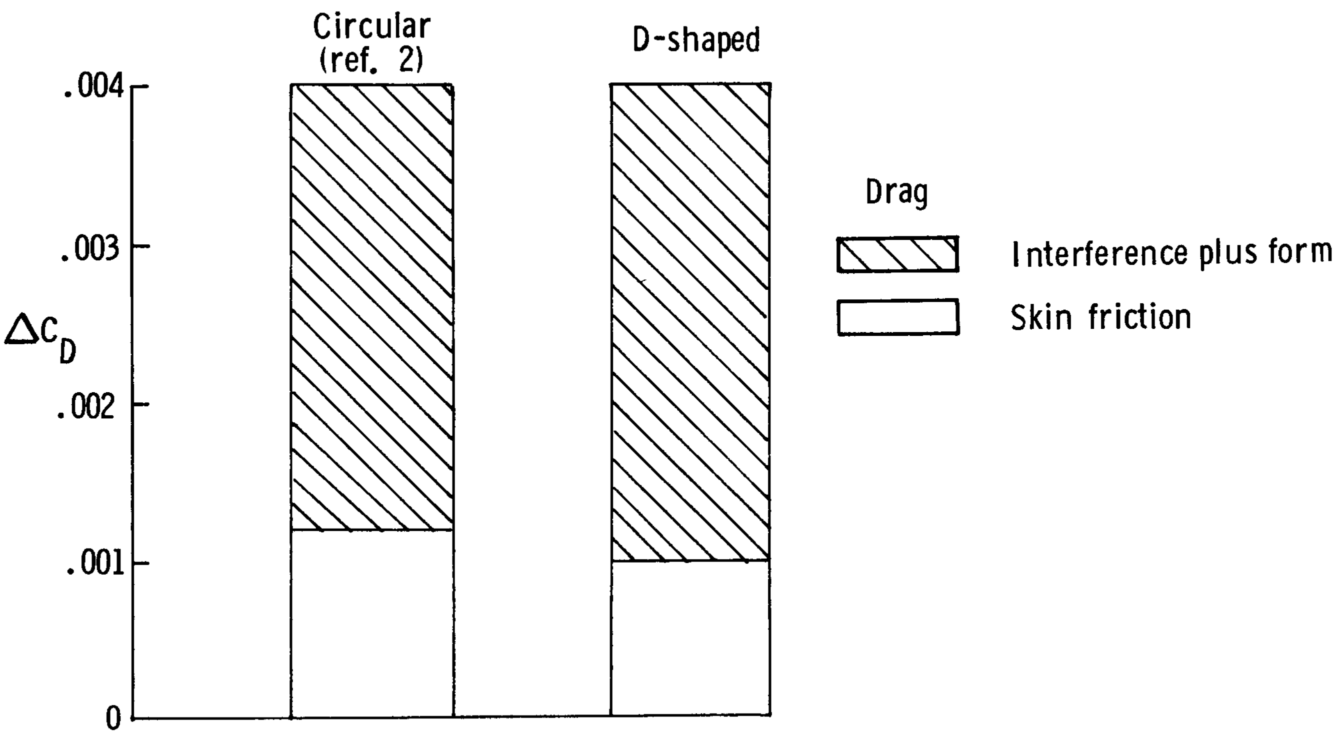

Figure 6. Installed drag coefficient at $M = 0.80$ and $C_L = 0.45$.

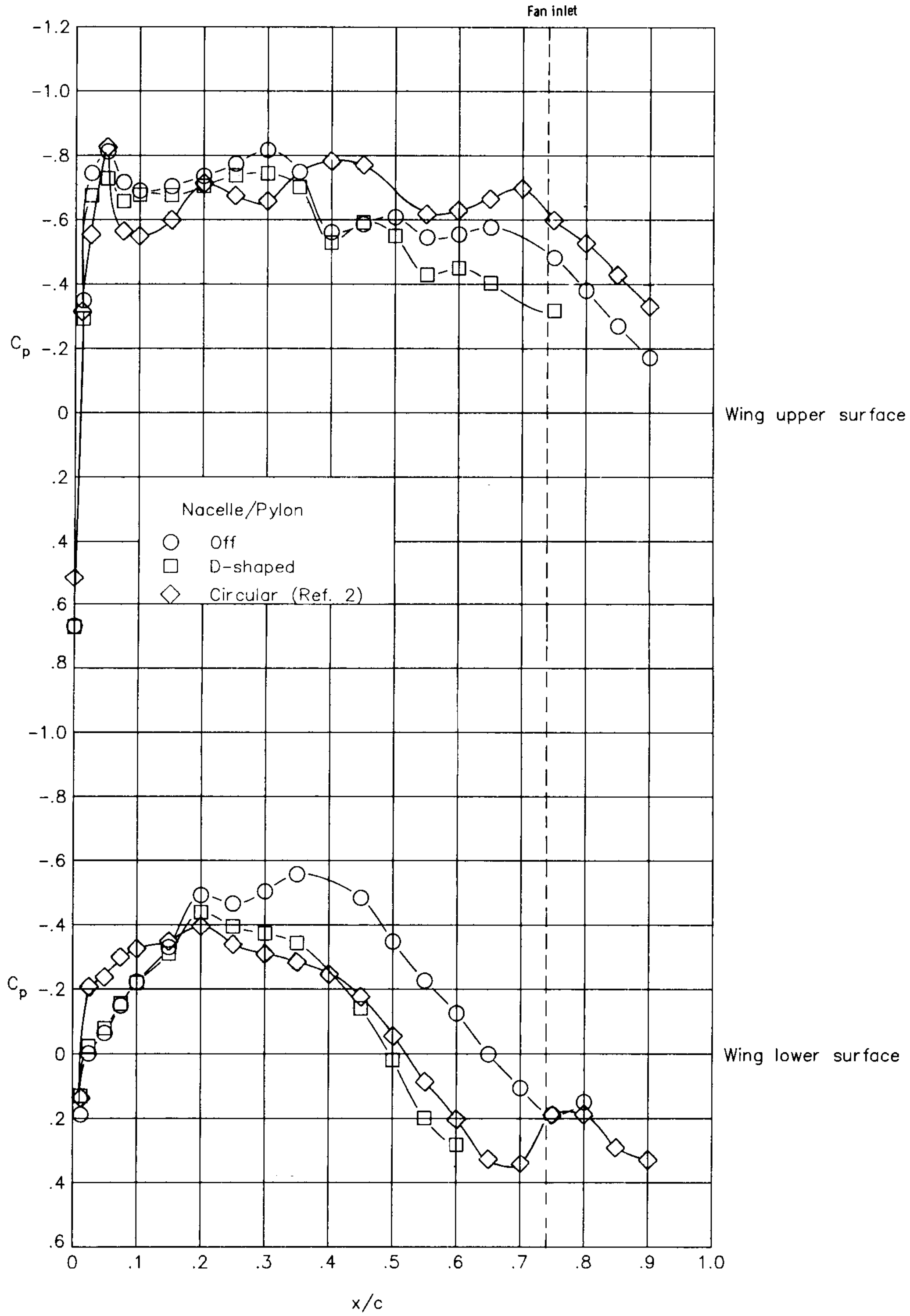

(a) $\eta = 0.328$.

Figure 7. Wing chordwise pressure distribution at $M = 0.80$ and $C_L = 0.43$.

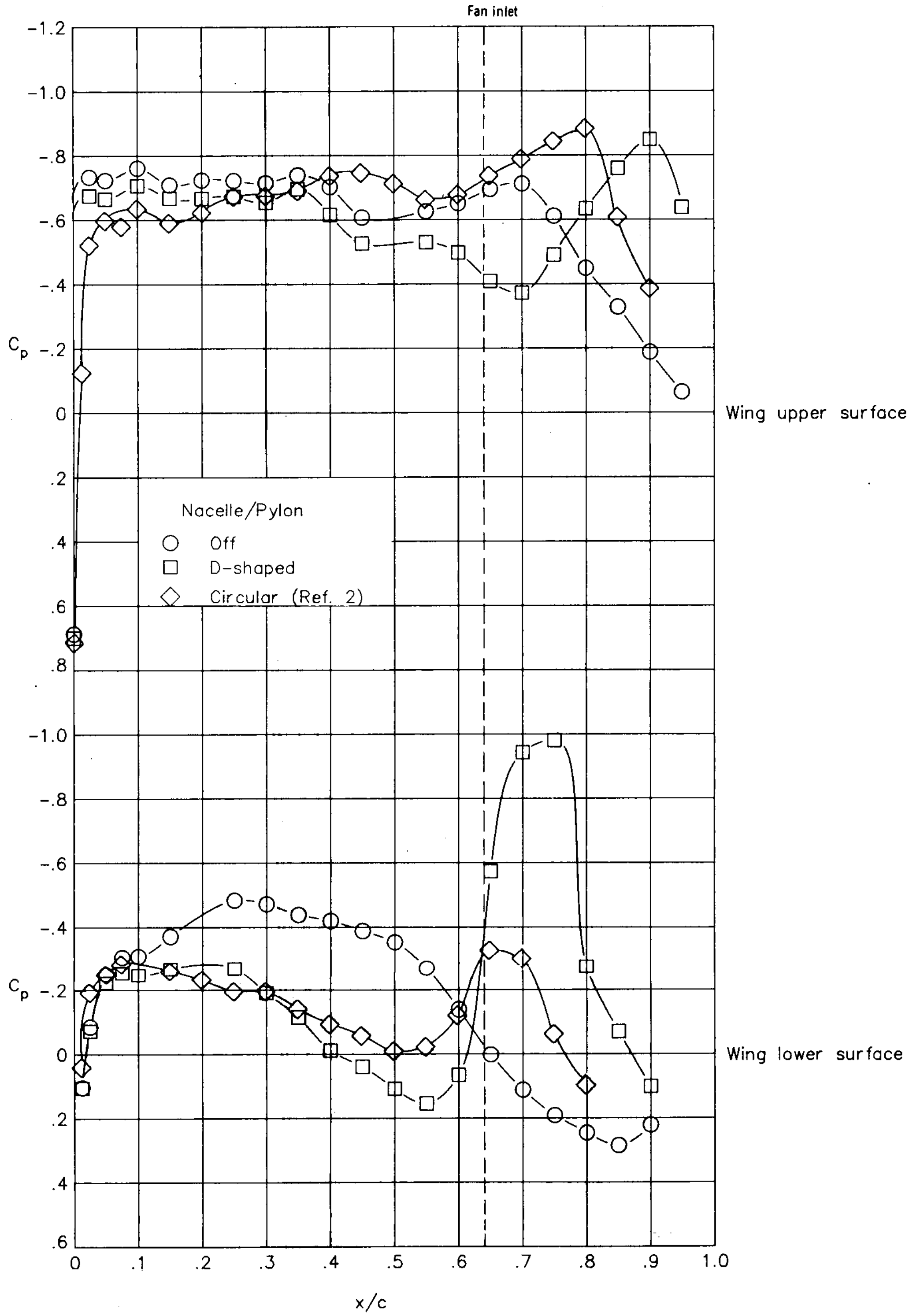

(b) $\eta = 0.440$.

Figure 7. Concluded.

NASA
National Aeronautics and Space Administration

Report Documentation Page

1. Report No.	2. Government Accession No.	3. Recipient's Catalog No.
NASA TM-4018		

4. Title and Subtitle	5. Report Date
Integration Effects of D-Shaped, Underwing, Aft-Mounted Separate-Flow, Flow-Through Nacelles on a High-Wing Transport	November 1987
	6. Performing Organization Code
7. Author(s)	8. Performing Organization Report No.
Milton Lamb, John R. Carlson, and Odis C. Pendergraft, Jr.	L-16342
9. Performing Organization Name and Address	10. Work Unit No.
NASA Langley Research Center Hampton, VA 23665-5225	505-68-91-06
	11. Contract or Grant No.
12. Sponsoring Agency Name and Address	13. Type of Report and Period Covered
National Aeronautics and Space Administration Washington, DC 20546-0001	Technical Memorandum
	14. Sponsoring Agency Code

15. Supplementary Notes

16. Abstract

An experimental investigation has been conducted in the Langley 16-Foot Transonic Tunnel at free-stream Mach numbers from 0.70 to 0.82 and angles of attack from $-3.0°$ to $4.0°$ to determine the integration effects of D-shaped, underwing, aft-mounted, separate-flow, flow-through nacelles on a high-wing transonic transport configuration. The results showed that the aft-mounted nacelle/pylon produced an increase in lift over that of the wing-body configuration by pressurizing much of the wing lower surface in front of the pylon. For the D-shaped nacelle, a substantial region of supersonic flow over the wing, aft of the lip of the nacelle, cancelled the reduction in drag caused by the increase in pressures ahead of the lip, to increase interference and form drag compared with a similar circular-shaped nacelle. The installed drag of the D-shaped nacelle was essentially the same as that of an aft-mounted circular nacelle from a previous investigation.

17. Key Words (Suggested by Authors(s))	18. Distribution Statement
Nacelle/pylon wing integration Transonic transport Separate flow, flow-through nacelles D-shaped, aft-mounted nacelles	Unclassified—Unlimited Subject Category 02

19. Security Classif.(of this report)	20. Security Classif.(of this page)	21. No. of Pages	22. Price
Unclassified	Unclassified	22	A02

NASA FORM 1626 OCT 86 NASA-Langley, 1987

For sale by the National Technical Information Service, Springfield, Virginia 22161-2171